



HAL
open science

Monte Carlo Aggregation Code (MCAC) Part 2: Application to soot agglomeration, highlighting the importance of primary particles

J. Morán, Jérôme Yon, Alexandre Poux, F. Corbin, F.-X. Ouf, A. Siméon

► To cite this version:

J. Morán, Jérôme Yon, Alexandre Poux, F. Corbin, F.-X. Ouf, et al.. Monte Carlo Aggregation Code (MCAC) Part 2: Application to soot agglomeration, highlighting the importance of primary particles. *Journal of Colloid and Interface Science*, 2020, 575, pp.274-285. 10.1016/j.jcis.2020.04.085 . hal-02563051

HAL Id: hal-02563051

<https://hal.science/hal-02563051v1>

Submitted on 14 Jan 2021

HAL is a multi-disciplinary open access archive for the deposit and dissemination of scientific research documents, whether they are published or not. The documents may come from teaching and research institutions in France or abroad, or from public or private research centers.

L'archive ouverte pluridisciplinaire **HAL**, est destinée au dépôt et à la diffusion de documents scientifiques de niveau recherche, publiés ou non, émanant des établissements d'enseignement et de recherche français ou étrangers, des laboratoires publics ou privés.



Distributed under a Creative Commons Attribution - NonCommercial - NoDerivatives 4.0
International License

Monte Carlo Aggregation Code (MCAC) Part 2: Application to soot agglomeration, highlighting the importance of primary particles

J. Morán^a, J. Yon^{a,*}, A. Poux^a, F. Corbin^a, F.-X. Ouf^b, A. Siméon^c

^a*Normandie Université, INSA Rouen, UNIROUEN, CNRS, CORIA, 76000, Rouen, France.*

^b*Institut de Radioprotection et de Sécurité Nucléaire (IRSN), PSN-RES, SCA, Gif-Sur-Yvette, 91192, France.*

^c*Université de Lille, CNRS, UMR 8518 -LOA -Laboratoire d'Optique Atmosphérique, 59000 Lille, France.*

Abstract

During the agglomeration of nanoparticles, notably soot, a change in both the flow regime (from free molecular to near continuum) as well as the change of agglomeration regime (from ballistic to diffusive) is expected. However, these effects are rarely taken into account in numerical simulations of particles agglomeration and yet, they are suspected to have an important impact on the agglomeration kinetics, particle morphologies and size distributions. This work intends to study these properties by using the MCAC presented in the preceding work (part 1) by focusing on the physical impact of varying the particle volume fraction and monomers size and polydispersity. The results show an important sensitivity of the kinetics of agglomeration, coagulation homogeneity and agglomerates morphology to the size of monomers. First, for smaller monomers diameters the agglomeration kinetic is enhanced and agglomerates are found to be more compact, characterized by larger fractal dimensions. Secondly, for large monomer diameters, fractal dimensions down to 1.67 can be found being therefore, smaller than the classical 1.78 for DLCA mechanism. One important conclusion is that variation in time of both the agglomeration and flow regimes has to be considered for a more accurate simulation of the agglomerates size distribution and morphology.

*Corresponding author.

E-mail address: yon@coria.fr

Keywords: Diffusive and Ballistic Agglomeration; Primary particles; Flow regime; Fractal Dimension; Soot

1. Introduction

The agglomeration of suspended nanoparticles is a phenomenon of great complexity but, also great common interest in both aerosol and colloid systems. In this process of agglomeration, particles naturally evolve into complex fractal-like morphology of polydisperse size consisting also of polydisperse primary particles. Eventually, depending on the physical conditions, particles may change the way they interact between each others and also the way they interact with the surrounding fluid. In other words, particles may undergo a change of flow regime and/or agglomeration regime, respectively. The flow regime is characterized by the classical fluid Knudsen number $\text{Kn}_f = \lambda_f/r_m$, where λ_f and r_m are the fluid mean free path and the particles mobility radius, respectively. When Kn_f tends toward 0, the relevant hydro/aerodynamic forces result from a continuous process (continuum regime) whereas, at large Kn_f it is related to discrete collisions with molecules (free molecular regime). As introduced by Pierce et al. [1], the agglomeration regime can be quantified by the nearest-neighbor Knudsen number $\text{Kn}_n = \lambda_p/r_n$, where λ_p is the particle persistent distance and r_n is the average nearest-neighbor distance. When Kn_n is high, the clusters agglomeration tends to become ballistically limited (i.e. BLCA) whereas when tending toward 0, it is diffusion limited (i.e. DLCA). Fig. 1 summarizes most of the

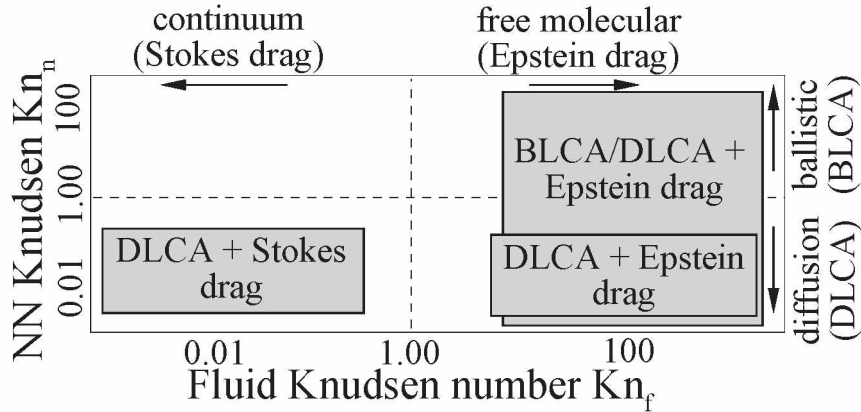


Figure 1: Different regimes of agglomeration and fluid flow studied in the literature. The nearest-neighbor Knudsen number is $\text{Kn}_n = \lambda_p/r_n$, where $\lambda_p = \sqrt{18D\tau}$ is the particle persistent distance [2] and r_n is the nearest-neighbor distance. The fluid Knudsen number is $\text{Kn}_f = \lambda_f/r_m$, where λ_f and r_m are the fluid mean free path and the particles mobility radius, respectively.

current simulations found in the literature as classified based on the above mentioned Knudsen numbers. Agglomeration has been commonly studied in the continuum flow regime for diffusion limited agglomeration (DLCA + Stokes drag) [3, 4]. Pierce et al. [1] studied the DLCA with an Epstein drag. Transition in the flow regimes (abscissa in Fig. 1) are complex due to the lack of models to calculate the friction coefficient of fractal agglomerates. In this context, some studies have treated both continuum and free molecular flow regimes separately [5]. Similarly, the ballistic limited (BLCA) and diffusion limited agglomeration (DLCA) are generally treated separately [3]. Only a few remarkable works considered a transition between both agglomeration regimes (vertical axis in Fig. 1) but, commonly in the free molecular flow regime, i.e. with an Epstein drag [6, 7].

To the author's knowledge, simultaneous transitions between both agglomeration and flow regimes have not been considered in the past except the remarkable attempt of Thajudeen et al. [8]. This work is based on Langevin Dynamics simulations by considering the agglomerate morphology, which is very accurate but computationally expensive. Also, in this study the influence of the nearest-neighbor distance was not systematically studied. In fact, they quantified the change of agglomeration regime (ballistic-diffusive) based on a diffusive Knudsen number to be discussed later. The Monte Carlo Aggregation Code, i.e. MCAC, developed and validated in the previous work (Part 1 [2]) enables to cover this gap with a reduced computational cost.

The present work aims to illustrate that caution has to be taken regarding the change in both regimes, because they impact the kinetics of agglomeration, size distribution and agglomerates morphology. On the one hand, when increasing the particles volume fraction (f_v) the r_n decreases and therefore Kn_n increases thus, the agglomeration becomes more ballistic and therefore an increase in the fractal dimension of agglomerates has been observed [9]. This is consistent with classical DLCA and BLCA regimes [3] but, in the present study, the transition between both regimes is continuous. On the other hand, when the primary particles diameter increases (for example during surface growth process), the flow regime evolves. In the context of soot simulation, agglomeration process is often restricted to the Epstein flow regime because of the large flame temperatures. Nevertheless, from nascent soot typically around 2-3 nm at flame temperatures to the mature primary particles around 30-40 nm eventually released to the atmosphere, the flow regime strongly evolves [10].

Another objective of the present study is to report and analyze the evolu-

tion of the coagulation kernels during the agglomeration process. Indeed, the Smoluchowski equation has been proved to be a powerful tool for modeling soot aggregation [11]. This equation follows the evolution of the particle number concentration as a function of time. To this end, $k(i, j)$ has to be known, i.e. the coagulation kernels determining the rate of collisions between particles i and j . In certain cases, especially for fractal agglomerates, this kernel is a homogeneous function, i.e. $k(\alpha i, \alpha j) = \alpha^\lambda k(i, j)$ where λ is the agglomeration kernel homogeneity parameter. This λ parameter is very important for the kinetics of agglomeration and the resulting self-preserving particles size distribution [12]. It has been proposed λ to be dependent on both the fluid Knudsen number and the nearest-neighbor Knudsen number [1, 6], however, these relations are not well understood especially in the transition regime. Considering its simplicity, the scaling hypothesis is widely used to obtain λ [3, 13, 14, 15] however, its accuracy is rarely discussed [16]. In the present work, a robust and more direct method for determining λ is proposed.

2. Numerical simulations

The algorithm used here has been introduced in the preceding work [2] and therefore, it is briefly described here. Agglomeration of initially monodisperse or polydisperse spherical primary particles is simulated by using a model inspired in the classical DLCA mechanism [3]. It starts with a total of $N_0 = 3200$ randomly placed monomers in a cubic box, ending when the average number of monomers per agglomerate is 100 [17]. Particles are displaced by following the individual positions in time, periodic boundary conditions are applied to avoid artificial effects due to the interaction between particles and the containing box. At each time iteration, particles are displaced individually in a random direction along the persistent distance $\lambda_p = \sqrt{18D\tau}$ (here D stands for the diffusion coefficient and $\tau = m/f$ is the momentum relaxation time, i.e. the ratio between the particle mass and friction coefficient). The corresponding physical time step is $\Delta t = 3\tau$. As discussed in [2], this time step ensures an accurate modeling of agglomeration by Monte Carlo simulations. If the displaced particle collides with a neighbor one, they irreversibly stick together otherwise, a new particle is randomly selected in an iterative fashion. The probabilities p_i for selecting and displacing a particle i are based on the individual time steps Δt_j of all the particles based on the relation $p_i = \Delta t_i^{-1} / \sum_j \Delta t_j^{-1}$. This ensures the whole population of particles evolving with a statistically equivalent residence time [2]. Both, the proba-

bilities of particles displacements and the persistent distances of individual particles depend on the friction coefficient. In order to take into account the possible change in flow regime due to agglomeration, the method proposed by Yon et al. [18] is used, consisting in a power law between the agglomerate friction coefficient and the number of constituting primary particles. This model gives a physical importance to the primary particle diameter and the number of monomers in the evaluation of the friction coefficient. Also, this model enables the determination of a mobility radius r_m of the agglomerates by considering their size, morphology and change in flow regime. Finally, when the initial number of monomers N_0 decreases by a factor of 8 then, each side of the box is duplicated and the number of agglomerates is increased 8 times by introducing periodic images of the existing ones [19].

In the present study, a constant primary particle bulk density $\rho_p = 1.8 \text{ g/cm}^3$ is considered, corresponding to soot particles with low organic content [20]. Three different monomers diameters are simulated, i.e. 1, 20 and 80 nm. Unless indicated, they all consist of monodisperse monomers ($\sigma_{geo,p} = 1$). For the case of polydisperse monomers a lognormal distribution is considered ($\sigma_{geo,p} = 2$). They are suspended in air at the temperature of 1700 K and the pressure of 101.3 kPa, corresponding to flame conditions [21]. Three different volumes fractions are simulated, i.e. 1, 10 and 10^4 ppm. All the results are averaged over 10 different simulations and error bars reported in figures correspond to the 95% of confidence intervals.

3. Results and discussion

3.1. Agglomeration and fluid flow regimes

First, recalling that one of the main advantages of MCAC is to consider the time evolving agglomeration regime (nearest-neighbor Knudsen number Kn_n) and time evolving fluid flow regime (fluid Knudsen number Kn_f). $\text{Kn}_n = \lambda_p/r_n$ corresponds to the ratio between the average persistent distance and the average nearest-neighbor distance r_n [1]. It is calculated as $r_n = n^{-1/3} - 2r_{max}$ where n is the particle number concentration and r_{max} is the average maximum radius describing the agglomerate. The Kn_n represents the regime of agglomeration, i.e. diffusive or ballistic [1] indicated in the vertical axis of Fig. 2. $\text{Kn}_f = \lambda_f/r_m$ is evaluated as the ratio between the fluid mean free path and the average particle mobility radius corresponding to the horizontal axis in Fig. 2. Initially, particles consist of isolated primary particles (top right position for each individual case). The initial primary particle

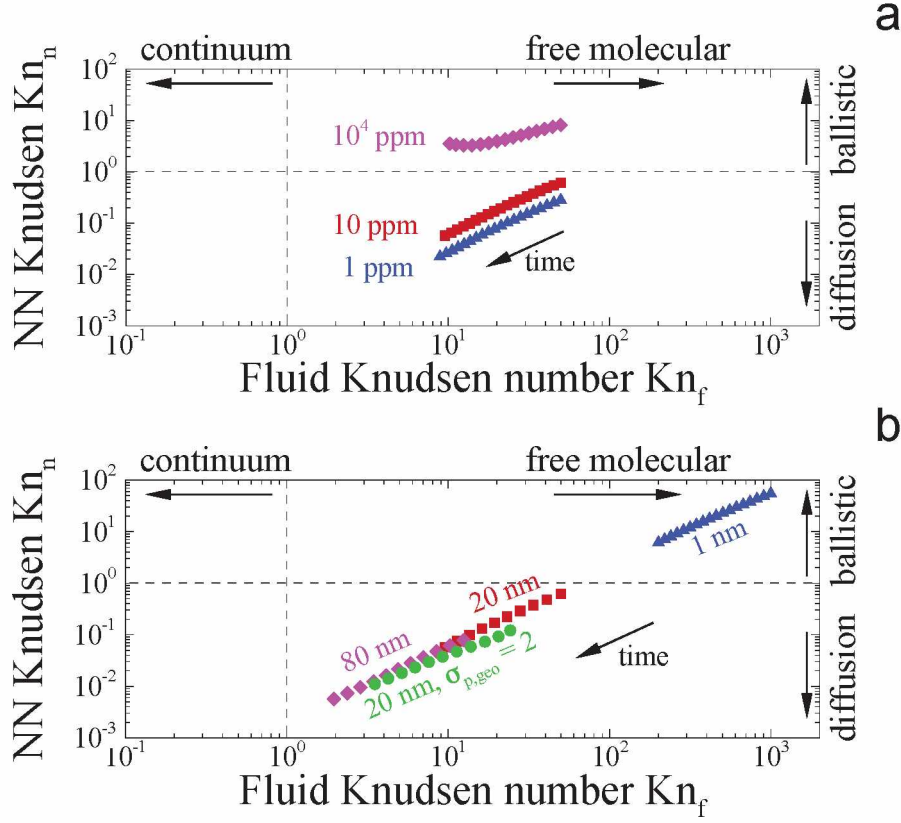


Figure 2: Different regimes of agglomeration and fluid flow for (a) different particles volume fraction and (b) different monomers diameters. The nearest-neighbor (NN) Knudsen number is $\text{Kn}_n = \lambda_p / r_n$, where $\lambda_p = \sqrt{18D\tau}$ is the particle persistent distance [2] and r_n is the average nearest-neighbor distance. The fluid Knudsen number is $\text{Kn}_f = \lambda_f / r_m$, where λ_f and r_m are the fluid mean free path and the particles mobility radius, respectively.

diameter and fluid thermodynamic properties determine the horizontal position of this starting point whereas, volume fraction and primary particle diameter determine the initial vertical position. As time progresses and agglomerates are growing, both Kn_n and Kn_f are decreasing. Fig. 2 clearly illustrates the ability of MCAC to consider the evolution of both Knudsen numbers and thus the transition from ballistic to diffusive and from free molecular to near continuum regimes. By comparing Fig. 2(a) and (b), it is observed that an acceptable variation of the monomers diameters (dealing with soot particles) seems to have a stronger influence on both regimes than

a large variation of the volume fraction. Except for the largest particles volume fraction, i.e. 10^4 ppm, the trends are generally related in a power law with a constant exponent. In the particular case of $f_v = 10^4$ ppm, the system never reaches the diffusive regime since the nearest neighbor distance is in competition with the fast increase of agglomerates size. This is interpreted as a trend towards gelation process [14], being out of the scope of this work.

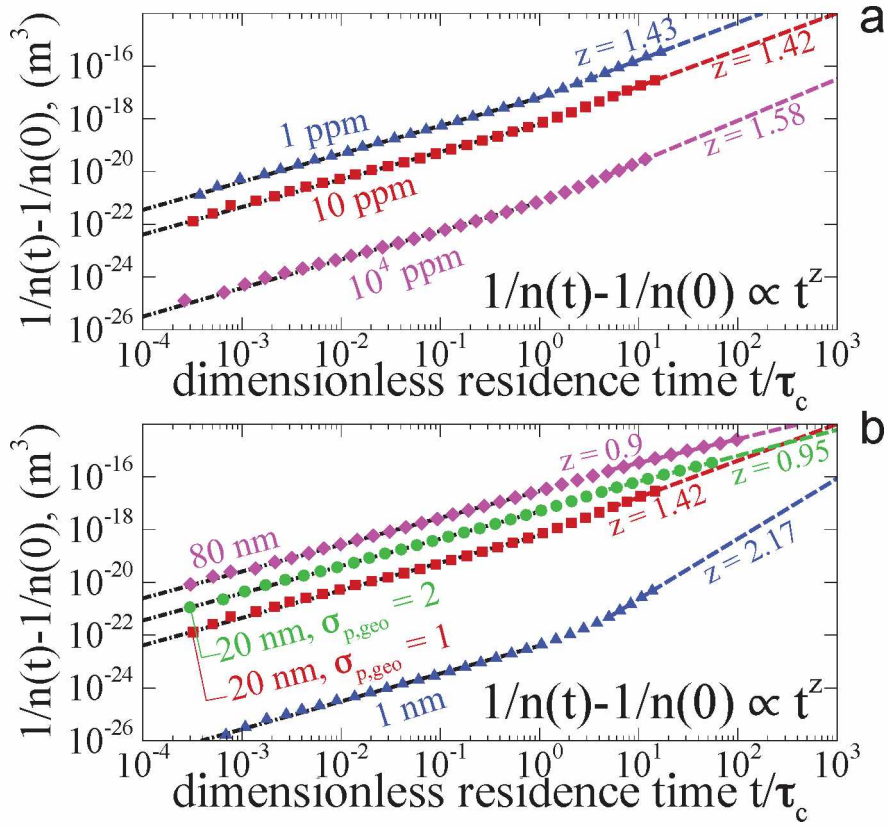


Figure 3: Inverse number concentration as a function of the normalized residence time. The τ_c stands for the characteristic time of coagulation.

3.2. Kinetics of agglomeration

Fig. 3(a-b) show the time evolution of the inverse number concentration $n(t)$ consisting in the number of particles divided by the volume of the containing box. Due to agglomeration, $1/n(t) - 1/n(0)$ is increasing in time. At

short times, when particles are small enough to be treated as spheres, the behavior is linear as predicted by coalescing spheres theory [22] (represented by black dash-dotted lines, i.e. $1/n(t) - 1/n(0) = (t/\tau_c)^z$ with $z = 1$). Also, Fig. 3(a-b) show a change of amplitude of the linear behavior at short times depending on f_v and d_p . This is related to a change of the characteristic time of coagulation τ_c . On the one hand, τ_c is calculated as the exponential of the intercept from the log-log plot of $1/n(t) - 1/n(0)$ as a function of time for very short times (where $z = 1$). The calculated values are reported in Table 1 and compared with the theoretical ones (τ_c^{sph}). The latter is determined as $\tau_c^{\text{sph}} = 2/(k_0 n_0)$ where, $n_0 = n(0)$ is the initial number concentration and k_0 is the coagulation kernel of coalescing spheres taking into account the change in flow regime [23], calculated based on initial monomers diameters. Both, τ_c^{sph} and τ_c are in the same order of magnitude except for the largest volume fraction (i.e. 10^4 ppm or 1%). Indeed, for that case, k_0 is no longer accurate to predict real coagulation efficiency and therefore the coagulation kernel is normally corrected by an enhancement factor not considered here [5, 24, 25]. The accordance of $z \rightarrow 1$ and $\tau_c \approx \tau_c^{\text{sph}}$ ensures a reliable simulation of the agglomeration kinetics by MCAC, at least for short times. For larger times

Table 1: Parameters for the analysis of agglomeration kinetics (kinetics exponent z). Also, the calculated and theoretical characteristics times of coagulation (for coalescing spheres), i.e. τ_c and τ_c^{sph} , respectively are indicated.

Case	short times		long times
	τ_c (μs)	τ_c^{sph} (μs)	z
f_v (ppm)			
1	1191	1262	1.43
10	107	126	1.42
10^4	0.06	0.13	1.58
d_p (nm)			
80	4550	4784	0.90
20	107	126	1.42
20 ($\sigma_{p,geo} = 2$)	505	—	0.95
1	0.03	0.07	2.17

corresponding to larger particles, due to the agglomerates morphology, the behavior tends to a power law $1/n(t) - 1/n(0) = (t/\tau_c)^z$, where z is the kinetic exponent that may be different of 1, and its value depends on the agglomeration and flow regimes [1, 5]. These values are displayed in Fig. 3(a-b)

and reported in Table 1. Kinetics of agglomeration is enhanced (z increases) when increasing the volume fraction or decreasing the monomers diameters. The largest value is found for $d_p = 1$ nm, which corresponds to a ballistic agglomeration (the largest Kn_n in Fig. 3(b)). This is in very good agreement with Pierce et al. [1] who reported an asymptotic value of $z = 2.2$ in this regime compared to 2.17 found in the present study. When decreasing Kn_n in Fig. 3, it corresponds to a general decrease of z , which appears to be more sensitive to the change of agglomeration regime.

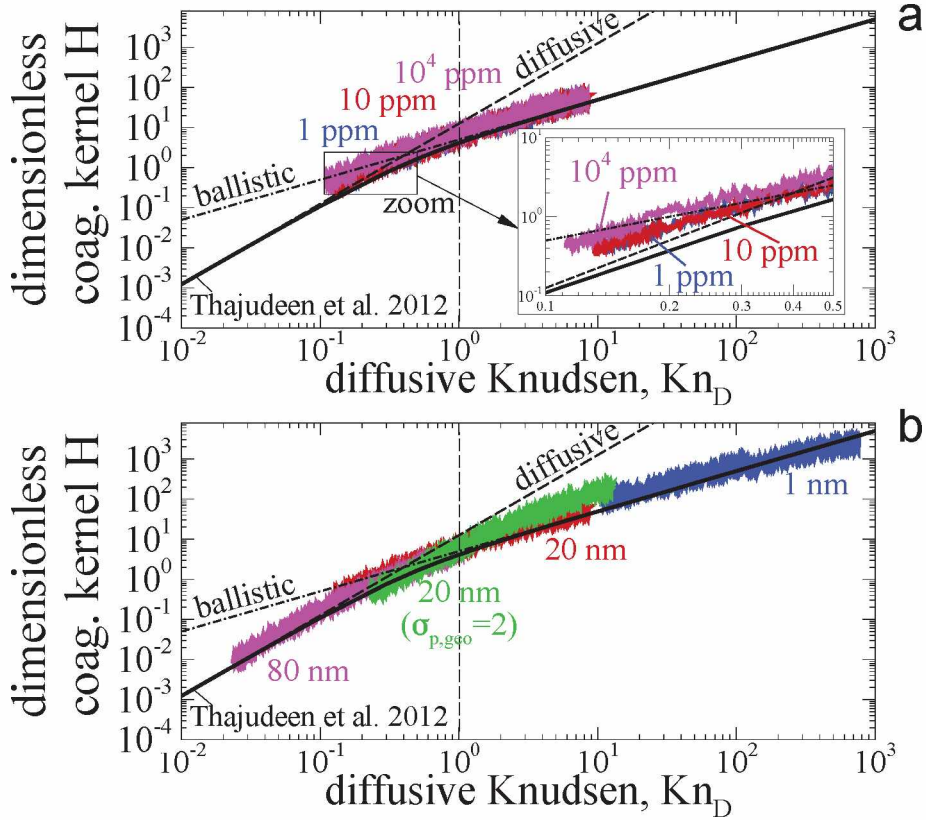


Figure 4: Dimensionless coagulation kernel H as a function of the diffusive Knudsen number for (a) different particles volume fraction and (b) different monomers diameters. H are obtained from eq. (1) by numerical differentiation of $k_{ii} = 2dn^{-1}/dt$ as a function of the diffusive Knudsen number compared with the results of Thajudeen et al. 2012 [26].

3.3. Coagulation kernels

As explained in the introduction, an important input parameter for Population Balance Equation in order to evaluate the evolution of the particles size distribution is the coagulation kernel ($k(i, j)$, i.e. the rate of collisions between particles consisting of i and j monomers). Fig. 4(a-b) report the dimensionless coagulation kernel H for monodisperse particles as formulated by Thajudeen et al. [26],

$$H = \frac{k_{ii} m_i \pi^2 R_{s,ii}}{f_i P A_{ii}^2}, \quad (1)$$

where k_{ii} , m_i and f_i are the coagulation kernel, mass and friction coefficient respectively. The symbols in the figure correspond to the k_{ii} obtained from the present simulation based on the local slopes of Fig. 3(a-b) ($k_{ii} = 2dn^{-1}/dt$ as proposed by Heine et al. [24]). Mass and friction coefficients are evaluated from the MCAC simulations. Also, $R_{s,ii}$ and PA_{ii} are the Smoluchowski radius and projected area, respectively, both are calculated based on the fractal dimensions reported later in this work (see Fig. 7) and the expressions proposed by [26]. All the above mentioned properties are evaluated based on population average values. In order to compare the current results (symbols) with the empirical relation proposed by [26] (continuous solid curves), the results are plotted as a function of the diffusive Knudsen number as introduced by the same authors and calculated as follows,

$$\text{Kn}_D = \frac{(2m_i k_B T)^{1/2} \pi R_{s,ii}}{f_i P A_{ii}}, \quad (2)$$

where k_B is the Boltzman constant. This Knudsen number has the same physical meaning than Kn_n used in the present study but, it is limited to a diluted system. As can be seen in Fig. 4(a-b) for all the simulated cases, a very good accordance is found between the present results and those by Thajudeen et al. [26] even if the considered range of primary particle diameters and volume fraction is huge. Nevertheless, a departure is observed for the high volume fraction case (10^4 ppm, Fig. 4(a)) explained by the deviation from the diluted assumption made by [26]. This illustrates that MCAC is able to reproduce reliable kernels from ballistic to diffusive regimes since Thajudeen et al. [26] obtained their results based on Langevin Dynamics simulations. But, MCAC is able to explore larger volume fractions and also

to take into account the primary particle polydispersity with a reduced computational cost. Also, contrarily to Thajudeen et al. [26], the agglomerate's morphology is not imposed in MCAC simulations. It is interesting to note in Fig. 4(b) that monomers polydispersity tends to increase the dimensionless coagulation kernels, especially for larger Kn_D .

3.4. Self preserving size distributions

It has been suggested in the literature that agglomerates attain a self-preserving size distribution (SPSD) in both free molecular and continuum flow regimes [27, 7]. This means that, after a given time, the dimensionless representation of the density of particles having a certain number of primary particles converges toward an asymptotic form [28]. This can be shown when agglomerate size parameter is normalized by its average value. Under this condition, the coagulation kernel $k(i, j)$ is a self-similar function, i.e. $k(\alpha i, \alpha j) = \alpha^\lambda k(i, j)$ where λ is the homogeneity coefficient and α is an arbitrary constant value [12]. Thus, λ can be used to monitor the SPSPD. Therefore, it is very interesting to study how this parameter is sensitive to a change in agglomeration or flow regimes. Usually, λ is determined by fitting the SPSPD [12, 1] or, as proposed by Dongen and Ernst [29], relying on the scaling hypothesis ($\lambda = 1 - 1/z$) based on the above mentioned kinetic exponent z . However, these approaches may be inaccurate and non robust. For these reasons, here an original and more robust method for determining λ and thus the agglomerate size distribution is proposed. Indeed, it is found that self preserving limit corresponds to a generalized Gamma distribution (please refer to [Appendix A](#)),

$$f(x) = \frac{(p/a^d)}{\tilde{x}\Gamma(d/p)} X^{d-1} \exp \left[- \left(\frac{X}{a} \right)^p \right], \quad (3)$$

where $f(x)$ is the probability density function. Here, x corresponds to one of the four size parameters considered in the present study as indicated in Table 2. In this equation, $\Gamma(z) = \int_0^\infty t^{z-1} e^{-t} dt$ is the Gamma function, p is a dimension parameter, $a = (1 - \lambda)^{-1/p}$, $d = p(1 - \lambda)$, and $X = x/\tilde{x}$ is a dimensionless size where $\tilde{x} = (\bar{x}^p)^{1/p}$. In addition to this generalized analytical expression of the SPSPD, an analytical expression of the q -moment of the generalized SPSPD is provided in [Appendix B](#). In Eq. (4), it is particularly reported the q -moment of the volume equivalent diameter $d_v = (6v/\pi)^{1/3}$

Table 2: Parameters for the generalized SPSD given by eq. (3).

Size descriptor	x	p
number monomers	N_p	1
volume eq. diameter	d_v	3
gyration diameter	d_g	D_f^a
mobility diameter	d_m	D_{fm}^b

^a Gyration diameter based on mass fractal dimension.

^b Mobility diameter based fractal dimension (scaling exponent).

distribution,

$$\overline{d_v^q} = \tilde{d}_v^q \frac{\Gamma(1 - \lambda + q/3)}{(1 - \lambda)^{q/3} \Gamma(1 - \lambda)}, \quad (4)$$

In the present work, it is proposed to evaluate the homogeneity coefficient λ based on a new and robust method. It consists in solving Eq. (4), for the first ($q = 1$) and second ($q = 2$) moments of the volume equivalent diameters distribution, to obtain the corresponding homogeneity coefficients. They are denoted as λ_{M1} and λ_{M2} , respectively, and results are presented in Fig. 5 with respective filled and empty symbols. For initially monodisperse monomers and for times lower than the time-lag for SPSD (found to be in average $5\tau_c$ or equivalent $\overline{N_p} = 20$, and represented by the gray zone in this figure), both, λ_{M1} and λ_{M2} are very different showing that SPSD cannot be used to model the actual particle size distribution. However, for larger times (or larger $\overline{N_p}$) both parameters generally converge well toward a common value evolving in time suggesting that particles size distributions are quasi self-preserving all along the agglomeration process. The range of observed values of λ for larger agglomerates is between -0.5 and 0.5, in the acceptable physical range discussed by Pierce et al. [1].

In order to evaluate the impact of the flow regime, the case of $d_p = 80$ nm and $f_v = 10$ ppm is again simulated, for which $\lambda = -0.5$ (pink symbols) by forcing the drag force to stay in the Epstein regime all along the agglomeration process to serve as a reference “classical” DLCA-Epstein scheme (black symbols, labeled DLCA in the figure). Note that the reference DLCA case is much more stable in term of λ than when the flow regimes is naturally evolving. Also, an asymptotic and different value is quickly reached. This highlights the importance of considering the natural evolution

of the flow regime. This is confirmed by the observed important role played by d_p as shown in Fig. 5(b), which is a key parameter for evaluating the friction coefficient and its dependence on the fluid regime. In comparison, the role played by f_v seems to have less relative impact.

The case of initially polydisperse monomers is represented by green circles symbols in Fig. 5(b). For short times both, λ_{M1} and λ_{M2} do not differ considerably. As discussed later and as proposed in the literature, the SPSD is not very different than a lognormal distribution [30, 31]. These parameters, attain the same value than the corresponding monodisperse case (with the same monomers geometric mean) but, the convergence is reached for larger agglomerate size ($\overline{N_p} \sim 70$). This is consistent with the results of Goudeli et al. [32] who showed by DEM simulations that agglomeration kernels become independent on the initial monomers polydispersity for large enough residence times. It is also consistent with Friedlander [22] who found the attained SPSD, characterized here by λ , to be independent on the initial particle size distribution. Because the SPSD is found to be relatively more influenced by the monomers diameters than particles volume fraction, Fig. 6(a-c) report the corresponding asymptotic SPSD obtained as a function of the dimensionless volume equivalent diameter, gyration and mobility diameters, respectively. To avoid overloading the figure, direct evaluation of the size distribution is reported in symbols only for the reference case (i.e. $d_p = 20$ nm) whereas, continuous curves correspond to the theoretical self-preserving functions (Eq. 3) evaluated with the final λ_{M1} found in Fig. 5, i.e. when $\overline{N_p} = 100$. First, a good agreement with the theoretical expression for the reference case is observed. This confirms the size distribution corresponds well to a SPSD. Secondly, the smaller the primary particle diameter, the wider becomes the distribution. This is also found with larger f_v (not presented here) indicating that ballistic and free molecular flow regimes are characterized by wider agglomerate size distributions. This result is in agreement with coalescing spheres for all regimes [27] and with agglomerates in the asymptotic regimes [7]. It is worth to highlight the ability of MCAC to simulate the quasi-SPSD in the transition regime. Finally, it can be seen the ability of MCAC to simulate the quasi-SPSD as a function of different size parameters. Modal diameters and standard deviations seem more different for gyration diameters than mobility or volume equivalent diameters. However, the size distribution expressed in mobility diameter does not converge exactly towards a lognormal size distribution (dashed red line in Fig. 6(c)) as experimental measurements usually report. This discrepancy

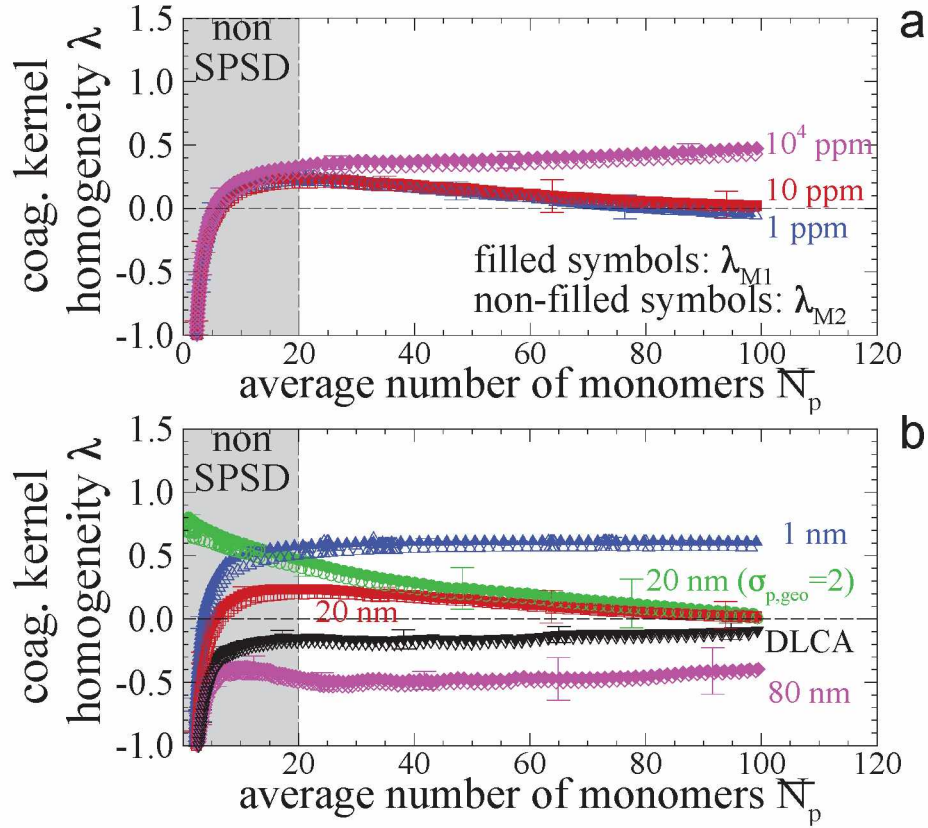


Figure 5: Coagulation kernel homogeneity coefficients for (a) different particles volume fraction and (b) different monomers diameters. Calculated from the first (λ_{M1} , filled symbols) and second (λ_{M2} , non-filled symbols) moments of the volume equivalent diameter distributions.

may be related to some physical phenomena not considered in the present Monte Carlo approach (for example, interaction potentials, surface growth or thermophoretic forces). Noting also that the simulated agglomerates are simplified in terms of morphology (one point contact spheres) compared to real soot particles as experimentally seen in TEM images [33, 34].

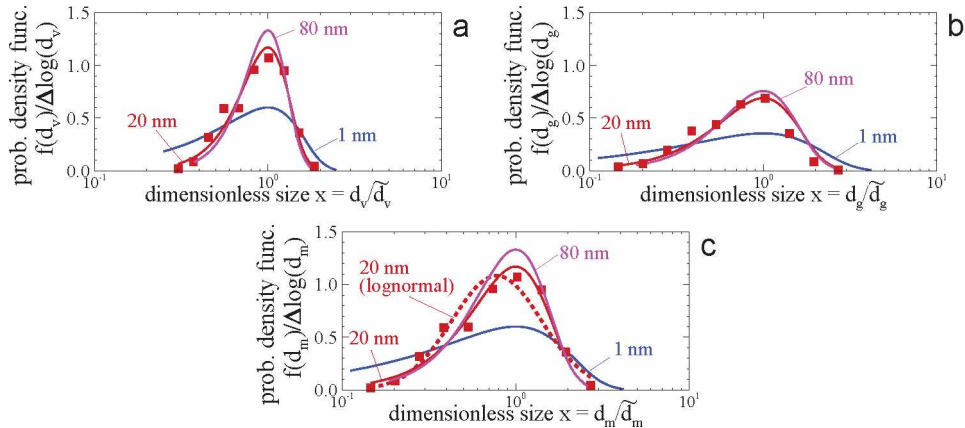


Figure 6: Asymptotic particles size distribution expressed in terms of (a) the volume equivalent diameter, (b) the diameter of gyration and (c) the mobility diameter.

3.5. Agglomerates morphology

The morphology of agglomerates is described by the population based fractal dimension D_f and prefactor k_f obtained based on the fractal law,

$$\frac{v_a}{v_p} = k_f \left(\frac{d_g}{d_p} \right)^{D_f} \quad (5)$$

where v_a/\bar{v}_p is the ratio between the agglomerate volume and the average monomers volume (corresponding to the number of primary particles N_p), d_g is the diameter of gyration and \bar{d}_p is defined here as the numerical average monomers diameter. Note that, there is no strict rule for using the fractal law when dealing with polydisperse primary particles [35, 36]. Defining differently the representative primary particle radius affects the so determined fractal prefactor but, not the fractal dimension. Also, the fractal law has been considered to be valid only for agglomerates large enough (typically $\bar{N}_p > 20$). When plotting in log-log plot N_p as a function of d_g/\bar{d}_p , a linear fit easily provides D_f and k_f . This procedure is repeated in the present study at each time iteration during the agglomeration process. The results are reported in Fig. 7(a-b) as a function of the mean number of primary particles per agglomerate. The filled symbols represent the fractal dimension (left vertical axis) whereas, empty symbols refer to the fractal prefactor (right vertical axis). The practical use of the fractal law is limited to constant k_f and D_f . It is clearly observed that this is not the case, in particular for $\bar{N}_p < 20$,

in agreement with the results obtained by Lazzari et al. [37]. Please note this limit is qualitative and values between 15 to 30 can be found in the literature [38, 39]. In this context, smaller particles are considered as non-fractals. Note, this method for determining k_f and D_f does not enable to converge to $D_f \rightarrow 3$ when $N_p \rightarrow 1$. Additionally, the current fractal dimension is different from the average one reported in the literature [7, 40, 39], this is inherent to the fitting method and to the definition of the fractal law.

In Fig. 7(a), an increase in the asymptotic fractal dimension as a function of particles volume fraction is observed, this is in agreement with previous studies [41, 42, 9, 37]. This is because agglomeration becomes more ballistic. Nevertheless, for soot agglomeration processes, such high volume fractions may be not common. Furthermore, the observed variation of D_f is not large (between 1.80 and 1.88). Thus, it is unlikely that this parameter alone can explain the variability of the fractal dimensions found in the literature [33]. Fig. 7(b) shows the more influencing effect of the primary particles diameter (D_f between 1.62 to 1.86). First, it is very remarkable that this value decreases when increasing the monomer diameters. The present results seems to indicate that primary particle diameter, that plays an important role in the evaluation of the drag force (see Eq. (2) in the preceding work [2]) and therefore, due to the change in flow regime, has a significant impact on soot morphology. This dependence has been previously observed experimentally for agglomerates formed by DLCA mechanism however, not clear explanation has been given [43] before this work. Thus, small fractal dimension (down to 1.62) can result of the agglomeration of large monodisperse primary particles or containing at least a few large primary particles as seen in Fig. 7(a) for the polydisperse case $\sigma_{p,geo} = 2$ reported in green. The observed impact of polydispersity is in accordance with Eggersdorfer and Pratsinis [44] who reported a fractal dimension of 1.68 when $\sigma_{p,geo} = 2$ for particles generated by a DLCA mechanism in the free molecular flow regime (with an Epstein drag). As discussed before, the change in flow regime is evaluated by comparing the results with the reference DLCA-Epstein case (black inverted triangle symbols in Fig. 7(b)). In this case, an asymptotic fractal dimension of 1.77 is found. Therefore, taking into account the change in the flow regime may have a strong impact in the agglomerates morphology.

On the other hand, the evolution of k_f as a function of $\overline{N_p}$ can be interpreted as a morphological signature different than the fractal dimension [46]. Particles volume fraction does not strongly affect the prefactor meanwhile, primary particles diameter and polydispersity seems to have a stronger ef-

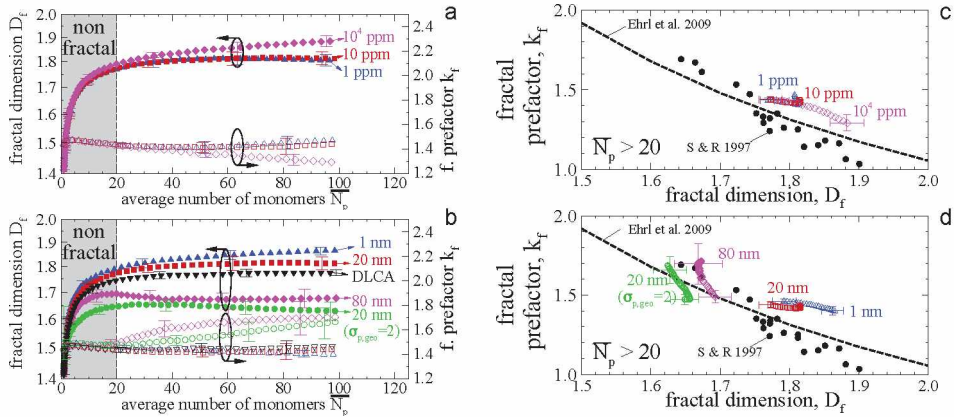


Figure 7: (a-b) Population based fractal dimension D_f and prefactor k_f as a function of the average number of monomers per agglomerate \bar{N}_p . (c-d) Fractal prefactor dependence on the fractal dimension for $\bar{N}_p > 20$ compared with Ehrl et al. [38] and Sorensen & Roberts [45].

fect. Fig. 7(a-b) seems to indicate an opposite trend in the relative variation of D_f and k_f . This is shown in Fig. 7(c-d) and compared with the literature [38, 45]. Only the parameters for $\bar{N}_p > 20$ are shown. The overall trend is that both parameters are inversely related, which is in accordance with the cited references. It is interesting to note that for both $d_p = 80$ nm ($\sigma_{p,geo} = 1$) and $d_p = 20$ nm ($\sigma_{p,geo} = 2$) the relative variation observed during the agglomeration process show a very different D_f compared with other simulated cases.

4. Conclusions

Monte Carlo Aggregation Code, MCAC, is used to simulate the agglomeration of soot particles by taking into account the change of both, flow and agglomeration regimes during agglomeration process. Monitoring both the nearest-neighbor (Kn_n) and fluid Knudsen number (Kn_f) is suggested to characterize the regimes of agglomeration and flow, respectively. This complements the suggestion of Thajudeen et al. [8] who proposed to monitor the diffusive Knudsen number instead of Kn_n .

On the one hand, when increasing the particles volume fraction, the kinetics of agglomeration is enhanced, which is consistent with previous results in the literature [15, 14]. In this context, an increase in the coagulation ker-

nel is also observed in accordance with previous studies [5, 24, 25]. Except in the case of $f_V = 10^4$ ppm, the dimensionless coagulation kernel is found to be in very good agreement with Thajudeen et al. [26]. Particles are also found to be more compact with a maximum $D_f = 1.86$ when $f_V = 10^4$ ppm.

On the other hand, when increasing the primary particles diameter, agglomeration kinetics is slower, particles size distribution is considerably different but always quasi self-preserving. Fractal dimension is found to be decreasing with primary particles diameter d_p . In particular, at flames conditions (1700 K of temperature and 1 atm of pressure), for monodisperse large monomers of size $d_p = 80$ nm, an asymptotic value of $D_f = 1.67$ is found when both agglomeration and flow regimes simultaneously evolve. This is lower than the typical 1.78 for agglomerates generated by purely DLCA mechanism [3]. In fact, for the same condition a $D_f = 1.77$ is attained when the agglomeration is simulated considering a classical DLCA-Epstein scheme, i.e. the drag force is imposed to be always in the Epstein regime.

The current numerical simulations suggest a decrease in the asymptotic fractal dimension as a function of the monomers diameters. This dependence has been suggested by reviewing experimental data by Wu et al. [43, 37], who highlighted the lack of explanation for this trend. Here, just considering the change of regime suffered by primary particles a possible explanation is proposed however, at this point, more complex phenomena (not considered here) such as, dipolar interactions, etc. cannot be discarded [37].

A new and robust method to determine the kernel homogeneity λ is introduced and discussed. It is based on the first and second moments of the analytical self-preserving particle size distribution [1, 6, 12]. This distribution is found to be a generalized gamma distribution. The homogeneity coefficient is also found to be very sensitive to the primary particle diameter and less sensible to the volume fraction for the cases studied here. It is commonly an evolving value as agglomeration progresses however, when $\overline{N}_p > 20$ its variation is not very large suggesting a quasi SPSD.

MCAC has been implemented in c++, and it will be publicly available in the following link <https://gitlab.coria-cfd.fr/MCAC/MCAC>.

Acknowledgments

This work is financed by ANR ASTORIA (N° ANR-18-CE05-0015) and the Region of Normandy (project RIN Gaspropres).

Appendix A. The generalized self preserving size distribution

Oh and Sorensen [12] introduced the following Self-preserving particles size distribution as expressed in terms of the volume of aggregates,

$$n(v) = M_1 s_b^{-2} \phi(x), \quad x = v/s_b \quad (\text{A.1})$$

where $n(v)dv$ represents the number concentration of particles whose volume is between v and $v + dv$, and where $s_b = M_b/M_{b-1}$, considering M_b as the b -moment of the volume-based particles size distribution,

$$M_b = \int_0^\infty v^b n(v) dv \quad (\text{A.2})$$

Additionally, $\phi(x)$ corresponds to the time-invariant shape of the SPSD,

$$\phi(X) = AX^{-\lambda} \exp[-(b - \lambda)X], \quad (\text{A.3})$$

where $A = (b - \lambda)^{b-\lambda}/\Gamma(b - \lambda)$. Therefore, they finally arrived to the following expression by rewriting Eq. (A.1) considering $b = 1$,

$$n(v) = \frac{1}{v} \frac{(1 - \lambda)^{1-\lambda}}{\Gamma(1 - \lambda)} X^{1-\lambda} \exp[-(1 - \lambda)X], \quad X = v/\bar{v} \quad (\text{A.4})$$

This expression can be converted to a probability density function $f(v)$ by calculating,

$$f(v)dv = \frac{n(v)dv}{\int_0^\infty n(v)dv} \quad (\text{A.5})$$

$$f(v) = \frac{1}{\bar{v}} \frac{(1 - \lambda)^{1-\lambda}}{\Gamma(1 - \lambda)} X^{1-\lambda} \exp[-(1 - \lambda)X], \quad X = v/\bar{v} \quad (\text{A.6})$$

For any equivalent diameter x related to the volume of the aggregate according to the following expression,

$$v = \alpha x^p \quad (\text{A.7})$$

where α and p correspond to a prefactor and exponent, respectively. Now, considering the probability to find a particle with a volume between v and

$v + dv$ is the same as the probability to find a particle with an equivalent diameter between x and $x + dx$, i.e. $f(v)dv = f(x)dx$ therefore,

$$f(x) = f(v)\alpha p x^{p-1}, \quad v = \alpha x^p \quad (\text{A.8})$$

Based on Eq. (A.6) and introducing $\tilde{x} = (\overline{x^p})^{1/p}$,

$$f(x) = \frac{p(1-\lambda)^{1-\lambda}}{\tilde{x}\Gamma(1-\lambda)} X^{p(1-\lambda)-1} \exp[-(1-\lambda)X], \quad X = (x/\tilde{x})^p \quad (\text{A.9})$$

Note that Eq. (A.9) is independent on the prefactor α . Finally, by introducing the following parameters $a = (1-\lambda)^{-1/p}$ and $d = p(1-\lambda)$ it is shown that Eq. (A.9) corresponds to a generalized Gamma distribution,

$$f(x) = \frac{(p/a^d)}{\tilde{x}\Gamma(d/p)} X^{d-1} \exp\left[-\left(\frac{X}{a}\right)^p\right], \quad X = (x/\tilde{x})^p \quad (\text{A.10})$$

Appendix B. q -moment of the generalized SPSD

The moment of order q of a distribution of a general probability density function $f(x)$ is,

$$\overline{x^q} = \int_0^\infty x^q f(x) dx, \quad (\text{B.1})$$

considering the $f(x)$ given by Eq. (A.10) the following expression is obtained,

$$\overline{x^q} = \tilde{x}^q a^q \frac{\Gamma\left(\frac{a+p}{q}\right)}{\Gamma(d/p)}, \quad (\text{B.2})$$

by replacing the previously defined parameters a and d ,

$$\overline{x^q} = \tilde{x}^q \frac{\Gamma(1-\lambda + p/q)}{(1-\lambda)^{q/p} \Gamma(1-\lambda)} \quad (\text{B.3})$$

References

- [1] F. Pierce, C. Sorensen, A. Chakrabarti, Computer simulation of diffusion-limited cluster-cluster aggregation with an Epstein drag force, *Physical Review E* 74 (2) (2006) 021411. doi:<https://doi.org/10.1103/PhysRevE.74.021411>.
- [2] J. Morán, J. Yon, A. Poux, Monte Carlo aggregation code (mCAC) part 1: Fundamentals, *Journal of Colloid and Interface Science* doi:<https://doi.org/10.1016/j.jcis.2020.02.039>.
- [3] P. Meakin, A historical introduction to computer models for fractal aggregates, *Journal of Sol-Gel Science and Technology* 15 (2) (1999) 97–117. doi:<https://doi.org/10.1023/A:1008731904082>.
- [4] S. Lazzari, M. Lattuada, Growth and aggregation regulate clusters structural properties and gel time, *The Journal of Physical Chemistry B* 121 (11) (2017) 2511–2524. doi:<https://doi.org/10.1021/acs.jpcb.6b12682>.
- [5] R. D. Mountain, G. W. Mulholland, H. Baum, Simulation of aerosol agglomeration in the free molecular and continuum flow regimes, *Journal of Colloid and Interface Science* 114 (1) (1986) 67–81. doi:[https://doi.org/10.1016/0021-9797\(86\)90241-9](https://doi.org/10.1016/0021-9797(86)90241-9).
- [6] W. R. Heinson, F. Pierce, C. M. Sorensen, A. Chakrabarti, Crossover from ballistic to Epstein diffusion in the free-molecular regime, *Aerosol Science and Technology* 48 (7) (2014) 738–746. doi:<https://doi.org/10.1080/02786826.2014.922677>.
- [7] E. Goudele, M. L. Eggersdorfer, S. E. Pratsinis, Coagulation–agglomeration of fractal-like particles: Structure and self-preserving size distribution, *Langmuir* 31 (4) (2015) 1320–1327. doi:<https://doi.org/10.1021/la504296z>.
- [8] T. Thajudeen, S. Deshmukh, C. J. Hogan Jr, Langevin simulation of aggregate formation in the transition regime, *Aerosol Science and Technology* 49 (2) (2015) 115–125. doi:<https://doi.org/10.1080/02786826.2015.1008971>.

- [9] R. Zahaf, S.-K. Kim, J. Shin, K. Park, T.-Y. Choi, D. Lee, Effect of volume fraction on transient structural behavior of aerosol particles using off-lattice kinetic monte carlo simulation, *Aerosol Science and Technology* 49 (12) (2015) 1242–1255. doi:<https://doi.org/10.1080/02786826.2015.1116681>.
- [10] M. L. Botero, N. Eaves, J. A. Dreyer, Y. Sheng, J. Akroyd, W. Yang, M. Kraft, Experimental and numerical study of the evolution of soot primary particles in a diffusion flame, *Proceedings of the Combustion Institute* 37 (2) (2019) 2047–2055. doi:<https://doi.org/10.1016/j.proci.2018.06.185>.
- [11] A. Jerez, J.-L. Consalvi, A. Fuentes, F. Liu, R. Demarco, Soot production modeling in a laminar coflow ethylene diffusion flame at different oxygen indices using a pah-based sectional model, *Fuel* 231 (2018) 404–416. doi:<https://doi.org/10.1016/j.fuel.2018.05.103>.
- [12] C. Oh, C. Sorensen, Light scattering study of fractal cluster aggregation near the free molecular regime, *Journal of Aerosol Science* 28 (6) (1997) 937–957. doi:[https://doi.org/10.1016/S0021-8502\(96\)00488-0](https://doi.org/10.1016/S0021-8502(96)00488-0).
- [13] G. Wang, C. Sorensen, Aggregation kernel homogeneity for fractal aggregate aerosols in the slip regime, *Aerosol Science & Technology* 34 (3) (2001) 297–306. doi:<https://doi.org/10.1080/027868201118313>.
- [14] P. Liu, W. R. Heinson, C. M. Sorensen, R. K. Chakrabarty, Kinetics of sol-to-gel transition in irreversible particulate systems, *Journal of colloid and interface science* 550 (2019) 57–63. doi:<https://doi.org/10.1016/j.jcis.2019.04.067>.
- [15] R. H. Ebini, C. M. Sorensen, Light scattering studies of the sol-to-gel transition in particulate systems, *Journal of colloid and interface science* 556 (2019) 577–583. doi:<https://doi.org/10.1016/j.jcis.2019.08.075>.
- [16] F. Leyvraz, Scaling theory and exactly solved models in the kinetics of irreversible aggregation, *Physics Reports* 383 (2-3) (2003) 95–212. doi:[https://doi.org/10.1016/S0370-1573\(03\)00241-2](https://doi.org/10.1016/S0370-1573(03)00241-2).